

11/12/2007

11/12/07

81450

INFLUENCE OF A SIMPLE HEAT LOSS PROFILE ON A
PURE DIFFUSION FLAME

Anjan Ray and Indrek S. Wichman*
Department of Mechanical Engineering
Michigan State University
East Lansing, MI 48824 USA
Phone: (517) 353-9180
Fax: (517) 353-1750
email: wichman@egr.msu.edu

*Corresponding author

ABSTRACT

The presence of soot on the fuel side of a diffusion flame results in significant radiative heat losses. The influence of a fuel side heat loss zone on a pure diffusion flame established between a fuel and an oxidizer wall is investigated by assuming a hypothetical $sech^2$ heat loss profile. The intensity and width of the loss zone are parametrically varied. The loss zone is placed at different distances from the Burke-Schumann flame location. The migration of the temperature and reactivity peaks are examined for a variety of situations. For certain cases the reaction zone breaks through the loss zone and relocates itself on the fuel side of the loss zone. In all cases the temperature and reactivity peaks move toward the fuel side with increased heat losses. The flame structure reveals that the primary balance for the energy equation is between the reaction term and the diffusion term. Extinction plots are generated for a variety of situations. The heat transfer from the flame to the walls and the radiative fraction is also investigated, and an analytical correlation formula, derived in a previous study, is shown to produce excellent predictions of our numerical results when an $O(1)$ numerical multiplicative constant is employed.

1. INTRODUCTION

The interaction between the structure of a diffusion flame (DF) and the flame radiation is quite complex. Soot is formed and oxidized in a diffusion flame as a consequence of a variety of physical and chemical processes. There are considerable uncertainties in the description of soot processes in a flame and the soot evolution mechanisms are not completely understood. Hence, the solution of the complex problem of diffusion flame - soot radiation interaction is very involved. The energy, species and soot volume fraction equations are all coupled and contain nonlinear source terms. In the present work we investigated the influence of a simple and contrived heat loss profile on a pure diffusion flame established between two diffusing walls of fuel and oxidizer.

The influence of heat transfer by radiation on flames has received significant attention in recent years [1-7]. Thermal radiation from a flame can occur from (1) radiation from the combustion gases at high temperature and (2) radiation from combustion generated particulates, i.e., soot. According to the calculations of Grosshandler and Modak [8] for soot volume fractions greater than 10^{-7} soot radiation is dominant. A review of pure diffusion flames without heat losses is presented first. In the following sections we define the problem geometry, describe the particular form of the heat loss profile used, formulate the conservation equations, briefly indicate the numerical method used and discuss the results.

In an ordinary diffusion flame the characteristic flow time is much greater than the characteristic chemical reaction time. This implies that the chemical reaction is much faster than the transport of species to the flame unless the flame is near or approaching the extinction stage. A pure diffusion flame is established when both oxidizer and fuel are transported to the flame

by means of diffusion only. No convective flow is present. Some important characteristics of pure diffusion flames have been discussed in [9], including an analysis of the detailed nature of the temperature and reaction rate profiles. It was observed that the maximum of the reaction rate profile usually will not coincide with the temperature profile maximum. The only exception is the symmetric flame for which the overall stoichiometric coefficient, $\phi (=vY_{FF}/Y_{OO})$, equals unity. This study shows, for a fuel-rich flame, that $Z_f \leq Z_r \leq Z_t$, i.e., the peak of the reaction rate profile (Z_r) lies between the Burke-Schumann flame location (Z_f) and the peak of the temperature profile (Z_t) for fuel rich conditions. For oxidizer-rich conditions, $Z_t \leq Z_r \leq Z_f$. It may be argued that in thin-flame limit all diffusion flames are "pure" diffusion flames because the mixture fraction transformation discussed in Williams, chap. 3 [10], produces an equation resembling $T_{zz} = |\underline{\nabla}Z|^{-2}\omega$, where $|\underline{\nabla}Z|$ is the magnitude of the mixture fraction gradient perpendicular to the flame. However, $|\underline{\nabla}Z|$ depends strongly on the heat and fluid flow conditions and in effect introduces a new parameter that must be accounted for in a complete analysis. Hence, though the value of $|\underline{\nabla}Z_f|$ (i.e., $|\underline{\nabla}Z|$ evaluated at the flame sheet) may be buried into a suitably redefined Damköhler number, it must of course be resurrected when later conducting a full examination of the problem.

Our goal in this work is to describe the response of a diffusion flame, when there is a zone of radiant soot-generated energy losses nearby, through the examination of a simplified model. A previously-generated theoretical correlation will be tested, and we shall, in addition, attempt to produce practical correlations of the total heat flux from the flame, the total (conductive plus radiative) energy flux to the surface, the drop in flame temperature due to radiant loss, etc. We shall not develop the full correlations here, but we indicate their dominant

behaviors. The complete correlations require numerical examination of all possible cases, something which was beyond the scope of this study.

2. THE MODEL

Figure 1 schematically depicts the problem geometry. The fuel wall and the oxidizer wall are located at $x=0$ and $x=L$, respectively. Both walls issue diffusive fluxes of the respective constituents. A diffusion flame is established between the two walls. A soot layer is assumed to exist on the fuel-side of the DF, consistent with experimental observations [11]. The walls have the ambient temperature T_o . There is no fuel on the oxidizer wall and no oxidizer on the fuel wall, the only possible other species at the walls being an inert element. The fuel and oxidizer mass fractions at the respective walls are specified to have values Y_{FF} and Y_{OO} as shown in Figure 1.

The combustion reaction is assumed to be a global, one-step chemical reaction of the form $F+\nu O\rightarrow(1+\nu)P$, where F denotes the fuel and O denotes the oxidizer. Methane is nominally the fuel under consideration and oxygen is the oxidizing specie, although real methane-oxygen reactions require of the order of 100 reaction steps and individual property choices for the separate species. The stoichiometric fuel-oxidizer mass ratio, ν , is four for the methane-oxygen combustion reaction. A suitable set of parameter values must be used to generate a reasonable range of Damköhler number and flame temperature values. The adiabatic flame temperature is given by $T_f=T_o+Q_F Y_{FF}/[C_p(1+\phi)]$, where Q_F is the heat release per unit mass of fuel from the combustion reaction and C_p is the specific heat of the mixture. The global stoichiometric coefficient, denoted by ϕ , is given by $\nu Y_{FF}/Y_{OO}$. However, the

use of the above formula produces unrealistically high adiabatic flame temperatures. Thus, the above equation for T_f was modified to produce a practical and reasonable range of adiabatic flame temperatures.

A set of realistic hydrocarbon combustion flame temperatures was obtained from the work of Wichman [12] for the analysis of flame spread over thermoplastics. The idea there was that the fuel mass fraction cannot reasonably be determined at the surface but a more-or-less generic flame temperature can still be calculated. This flame temperature varies only with the free-stream oxidizer mass fraction Y_{∞} . The value of Y_{FF} i.e., the fuel mass fraction in the hypothetical fuel stream for our present calculations was assumed to be 0.85. The oxidizer mass fractions (Y_{∞}) and the flame temperatures (T_f) are tabulated in Table 1.

A fourth order polynomial was fitted to the above data to obtain

$$T_f = 486.66 + 12230.85Y_{\infty} - 25728.64Y_{\infty}^2 + 25360.02Y_{\infty}^3 - 9323.0Y_{\infty}^4 \quad (1)$$

Using this expression, we generate points for a (Y_{∞}, T_f) plot.

We calculate Q_F by using the relation $Q_F = (T_f - T_o)C_p(1 + \phi)/Y_{FF}$ for $T_f = 2137K$, $Y_{\infty} = 0.211$, $Y_{FF} = 0.85$ and $T_o = 298K$. The calculated value of Q_F is 11959.43 kJ/kgK.

We now introduce a modified formula for the calculation of the flame temperature,

$$T_f = T_o + \frac{Q_F Y_{FF} f(Y_{\infty})}{C_p(1 + \phi)} \quad (2)$$

Next we calculate the values of the modification factor, $f(Y_{\infty})$, by using the above expression.

The calculated value of Q_F and the (Y_{∞}, T_f) data obtained using equation (1) were utilized for this purpose. The $f(Y_{\infty})$ data were as follows,

$$f=1.25\exp(-2.99Y_{\infty})+0.33 \quad (3)$$

Finally, we use the above expression for $f(Y_{\infty})$ to calculate T_f for any set of Y_{∞} and Y_{FF} values in equation (2). A plot of T_f versus Y_{∞} is shown in Figure 2. The Y_{FF} values corresponding to the different curves in the plot range from 0.25 to 1.0. The lowest curve is for $Y_{FF}=0.25$. The curves above are for $Y_{FF}=0.30, 0.35, 0.40$, etc. We note that for $Y_{FF}=0.25$ and 0.30 the peak flame temperature does not occur at $Y_{\infty}=1$; there is a slight local maximum in the range $0<Y_{\infty}<1$. For this reason we shall not use these curves. However, for higher values of Y_{FF} we do obtain temperature profiles whose maxima occur at $Y_{\infty}=1$. These profiles will be used. Also, we note that since we are interested in the effect of soot radiation on diffusion flames, we are not concerned with low values of Y_{FF} which do not produce significant amounts of soot. Hence, in our analysis, Y_{FF} values of 0.30 and lower are not used with reasonable physical justification.

The parameter values in the work of Tzeng et al. [13] were used in this article. The important values are shown in Table 2.

Here we write the equations and boundary conditions for conservation of energy and species. The energy conservation equation is

$$\rho C_p [T_t + u T_x] = (\lambda T_x)_x + Q_F \dot{\omega}_F - \frac{dq_R}{dx}, \quad (4)$$

with boundary conditions $T(x=0)=T_o$ and $T(x=L)=T_o$, where T_o is the temperature at the fuel and oxidizer walls, assumed to be 298 K. Here T is the temperature, ρ is the density, C_p is the specific heat of the mixture, λ is the thermal conductivity and u is the velocity. The

volumetric radiative heat loss term is $-dq_R/dx$ with units W/m^3 . The heat release due to combustion is Q_F and $\dot{\omega}_F$ is the reaction rate term. An Arrhenius type expression was assumed for the one-step irreversible reaction, so the reaction rate is $\dot{\omega}_F = \rho A Y_O Y_F \exp(-E/RT)$. The quantity A denotes the pre-exponential factor. The thermal conductivity is λ . The oxidizer mass fraction equation is

$$\rho[Y_{O_i} + uY_{O_i}] = (\rho D_O Y_{O_i})_x - v\dot{\omega}_F \quad (5)$$

with boundary conditions $Y_{O_i}(x=0)=0$ and $Y_{O_i}(x=L)=Y_{O_i\infty}$. Here, D_O is the mass diffusivity of the oxidizer. Similarly the fuel mass fraction equation is

$$\rho[Y_{F_i} + uY_{F_i}] = (\rho D_F Y_{F_i})_x - \dot{\omega}_F \quad (6)$$

with boundary conditions $Y_{F_i}(x=0)=Y_{F_iF}$ and $Y_{F_i}(x=L)=0$; D_F is the mass diffusivity of the fuel.

The above equations are now transformed to a mass coordinate system. The transformed coordinate is $Z=1-s/s_0$, where $s = \int_0^x \rho dx$ and $s_0 = \int_0^L \rho dx$. We note that $Z=1$ when $x=0$ and $Z=0$ when $x=L$. The coordinate Z happens to be identical to the mixture fraction coordinate for our simple problem. The following expressions hold for the above transformation:

$$\left. \frac{\partial}{\partial x} \right|_x = \left[-\frac{1}{s_0} ((\rho u)_0 - (\rho u)_x) + \frac{s}{s_0^2} ((\rho u)_0 - (\rho u)_L) \right] \left. \frac{\partial}{\partial Z} \right|_Z + \left. \frac{\partial}{\partial t} \right|_Z \quad (7)$$

and

$$\left. \frac{\partial}{\partial x} \right|_x = -\frac{\rho}{s_0} \left. \frac{\partial}{\partial Z} \right|_Z \quad (8)$$

Since we are considering a pure diffusion flame, $(\rho u)_{x=0} = (\rho u)_{x=L} = 0$, i.e., there are no

convective flows from the walls. Application of these operators to the energy and species equations and assuming $\rho\lambda$, ρ^2D_O , ρ^2D_F are constant, assuming the Lewis number is unity and $D_O=D_F$ and then introducing the nondimensional variables $\tau=(T-T_o)/(T_f-T_o)$,

$$y_O=Y_O/Y_{O\infty}, \quad y_F=Y_F/Y_{F\infty}, \quad \bar{s}=s/(\rho_o L) \quad \text{gives}$$

$$\tau_{\bar{t}} = \frac{1}{\bar{s}_o^2} \tau_{zz} + \bar{Q}_F D r + \frac{N_R}{\bar{s}_o} \frac{d\bar{q}_R}{dZ}, \quad (9)$$

$$y_{O_{\bar{t}}} = \frac{1}{\bar{s}_o^2} y_{O_{zz}} - \phi D r, \quad (10)$$

$$y_{F_{\bar{t}}} = \frac{1}{\bar{s}_o^2} y_{F_{zz}} - D r, \quad (11)$$

where $\bar{s}_o = s_o / (\rho_o L) = \int_0^1 \bar{\rho} d\bar{x}$ where $\bar{\rho} = \rho / \rho_o$ and $\bar{x} = x / L$. Also, r is the nondimensional reaction rate and N_R is a radiation number [14] evaluated as the ratio of the reference radiative and conductive fluxes, given by $N_R = q_{R,ref} / (\lambda_o (T_f - T_o) / L)$. The thermal conductivity at the reference condition is denoted by λ_o . The quantity D is the Damköhler number given by t_{ref} / t_{chem} , where the reference diffusion time is $t_{ref} = L^2 / \alpha_o$ and the characteristic chemical time is $t_{chem} = 1 / [A Y_{O\infty} \exp(-E/RT_p)]$. The nondimensional quantity \bar{q}_R is given by $q_R / q_{R,ref}$ where $q_{R,ref}$ is a reference radiative heat flux. The nondimensional heat release, \bar{Q}_F is given by $Q_F Y_{F\infty} / [C_p (T_f - T_o)]$ and equals $(1 + \phi)$ since the adiabatic flame temperature is defined as $T_f = T_o + Q_F Y_{F\infty} / [C_p (1 + \phi)]$. We note that in the prefactor multiplying the reaction term of equation (9) we do not utilize the temperature correction discussed previously. In addition, we have defined $\bar{t} = t / t_{ref}$. The nondimensional reaction term, r , is written in the form $r = y_O y_F \exp[-\beta(1 - \tau) / (1 - \alpha(1 - \tau))]$, where $\alpha = 1 - T_o / T_f$ and $\beta = E \alpha / (R_u T_p)$; E is the activation

energy and R_u is the universal gas constant. The quantity β is known as the Zeldovich number.

2.1 Infinite Reaction Rate (IRR) Solutions as Initial Conditions

Equations (9)-(11) are the governing conservation equations for τ , y_O and y_F for the case of finite rate chemistry. The equations become much simpler when the reaction rate is infinite. In this case, all fuel reaching the flame surface is consumed instantaneously, and similarly for the oxidizer. Thus no fuel exists on the oxidizer side and no oxidizer exists on the fuel side, i.e., $y_O y_F = 0$ on both sides of the flame. The energy equation can now be solved in two adjacent domains, the oxidizer side ($0 \leq Z \leq Z_f$) and the fuel side ($Z_f \leq Z \leq 1$) of the flame. The flame location is designated by Z_f . For our simple problem the mass coordinate Z coincides with the mixture fraction, a conserved scalar: this is a rare special case. In the absence of radiative losses the steady state energy equation becomes $\tau_{zz} = 0$. Since, at the flame $\tau = 1$, the solution of the steady state energy equation ($\tau_{zz} = 0$, since $N_R = 0$ and the reaction term can be excluded) for the infinite reaction rate (IRR) situation gives $\tau = Z/Z_f$ for $0 \leq Z \leq Z_f$ and $\tau = (1-Z)/(1-Z_f)$ for $Z_f \leq Z \leq 1$. Similarly, y_O and y_F can be solved for the infinite reaction rate situation and we get $y_O = (1-Z) - (1-Z_f)\tau$ for $0 \leq Z \leq Z_f$ and $y_F = Z - Z_f\tau$ for $Z_f \leq Z \leq 1$.

Next, we must evaluate Z_f the coordinate location of the IRR flame. As mentioned, Z is the mixture fraction coordinate, defined as $Z = (\phi y_F + 1 - y_O)/(\phi + 1)$. At the flame, y_O and y_F are both zero so that $Z_f = 1/(\phi + 1)$. With knowledge of Z_f the nondimensional temperature and species equations can all be determine exactly. The profiles so obtained are used as initial profiles for the numerical solution of the transient conservation equations (9)-(11).

2.2 Simple Heat Loss Profile

As shown in Wichman and Ray [14] the simplest model heat loss profile is the "top-hat" profile used therein. Because of the discontinuous derivatives at the edges of the top-hat profile, it is not as convenient for numerical reasons as a smooth and continuous heat loss profile. For primarily this reason, the profile that we shall use here is of the form of a $sech^2$ in mixture fraction space, viz.,

$$-\frac{d\bar{q}_R}{dZ} = sech^2(B(Z-Z_R)). \quad (12)$$

The location where the maximum of $-d\bar{q}_R/dZ$ occurs is denoted by Z_R . Figure 3 illustrates the nature of variation of the heat loss profile in mixture fraction space. We note that the maximum value of the profile is unity. We define the Z locations where the value of the function is 1% of its peak value as the two tails of the function, located respectively at locations we presently call Z_{R-} and Z_{R+} , with $Z_{R-} < Z_{R+}$. The maximum of the $-d\bar{q}_R/dZ$ profile occurs at $Z_R = (Z_{R-} + Z_{R+})/2$. The width of the loss zone is defined to be $\Delta Z_R = Z_{R+} - Z_{R-}$. The separation distance of the loss zone from the location of the ideal Burke-Schumann flame Z_f is given by $\Delta = Z_{R-} - Z_f$. In the subsequent analysis, we shall vary the thickness ΔZ_R as well as the separation distance Δ , in order to study the influence of the loss zone on the flame structure. The thickness of the loss zone can be chosen by selecting different values of the parameter B in equation (12).

From equation (9) we note that the radiative loss term is given by $(N_R \bar{s}_0) d\bar{q}_R/dZ$, and hence, another important way to modify the loss term is to experiment with the value of its

amplitude, N_R/\bar{s}_0 . We can choose different values of N_R the radiation number. The quantity \bar{s}_0 , given by $s_0/(\rho_0 L)$ is a by-product of the solution and for this reason is evaluated at each time step.

We recall that for the top-hat profile the integrated heat loss is $\int_0^1 (N_R/\bar{s}_0)(U(Z_{R-}) - U(Z_{R+}))dZ = N_R/\bar{s}_0 \Delta Z_R$. In this case the integrated heat loss is given by $s_0^{-1} \int_0^1 N_R \text{sech}^2[B(Z - Z_R)]dZ = N_R/(B\bar{s}_0) [\tanh B(1 - Z_R) + \tanh BZ_R]$. For large B this simplifies to $2N_R/\bar{s}_0/B + O(B^{-2})$, showing that the top-hat loss zone thickness ΔZ_R corresponds to $2/B$, or $B = 2/\Delta Z_R$. Consequently, in analytical formulae for the top-hat profile (see ref. [14]) we can substitute for ΔZ_R the value $2/B$ in order to test their correspondence to the *sech*² profile.

3. NUMERICAL SOLUTION

Equations (9), (10) and (11) were numerically solved with a the finite difference scheme. The nonlinear source terms were linearized using Newton's method. For each time step, iterations were used until the sum of normalized residuals became smaller than 1×10^{-6} . The transient conservation equations were integrated to steady state.

We utilize the ideal gas law to derive a relation between the temperature and density of the system. We can write $pV = (m/\bar{W})R_u T$ where p is the density and R is the gas constant for the mixture, given by $R = R_u/\bar{W}$. If we assume $p_0 R T_0$ to be the constant pressure of the system, then the introduction of $\alpha = 1 - T_f/T_f$ and $\tau = (T - T_0)/(T_f - T_0)$ results in the following important relation:

$$\frac{\bar{\rho}}{\rho} = \frac{1 - \alpha}{1 - \alpha(1 - \tau)} \quad (13)$$

We observe that when the temperature is that of the ambient, i.e., $T=T_o=298K$, then $\tau=0$ and $\bar{\rho}=1$, i.e., $\rho=\rho_o$. At the flame temperature (T_f) the nondimensional density is $\bar{\rho}=1-\alpha$ and consequently $\rho=(1-\alpha)\rho_o$.

Equations (9)-(11) indicate that in order to solve the τ , y_o and y_f equations, we need to evaluate \bar{s}_o at every time step. The quantity \bar{s}_o enters the analysis by virtue of the coordinate transformation $Z=1-\bar{s}/\bar{s}_o$. By differentiating both sides of this relation, we obtain $dZ/d\bar{x}=-\bar{\rho}/\bar{s}_o$, since $\bar{s}=\int_0^{\bar{x}}\bar{\rho}d\bar{x}$ and $\bar{x}=x/L$. Using the transformation relation between Z and \bar{x} , subject to the above mentioned boundary conditions, we get

$$\bar{s}_o = \frac{1}{\int_0^1 \frac{1}{\bar{\rho}} dZ}, \quad (14)$$

and the relation between the \bar{x} and Z coordinates can be written as

$$\bar{x} = \frac{\int_Z^1 (1/\bar{\rho}) dZ}{\int_0^1 (1/\bar{\rho}) dZ}. \quad (15)$$

On obtaining the solutions for τ , y_o and y_f equation (15) is used to transform the solutions back to the physical coordinate \bar{x} . Thus, \bar{s}_o can be evaluated once the $\bar{\rho}$ distribution is known. The normalized density $\bar{\rho}$ can be related to the τ distribution by virtue of equation (13). Hence, the expression for \bar{s}_o can alternatively be written as

$$\bar{s}_o = \frac{1}{\int_0^1 dZ + (\alpha/(1-\alpha)) \int_0^1 \tau dZ}. \quad (16)$$

Hence, on obtaining the τ profile we can determine the quantity \bar{s}_0 . When the temperature throughout the domain is the same as the ambient temperature T_o , then $\tau=0$ everywhere; by using equation (16), we obtain $\bar{s}_0=1$. If we next assume that the temperature everywhere in the domain is the adiabatic flame temperature T_f , then $\tau=1$ and $\bar{s}_0=(1-\alpha)$. Since the minimum and maximum values of temperature are T_o and T_f respectively, the quantity \bar{s}_0 must obey the limits $(1-\alpha)\leq\bar{s}_0\leq 1$.

4. RESULTS AND DISCUSSION

Figure 4 depicts the nondimensional temperature, τ , plotted as a function of the mixture fraction coordinate, Z , for different values of the radiation number, N_R for the particular parameter values shown in the title of the figure. The oxidizer and fuel mass fractions at the respective walls are $Y_{OO}=0.6$ and $Y_{FF}=0.8$. In our subsequent analysis we keep the same set of oxidizer and fuel mass fractions, and vary the location, width and intensity of the radiative loss zone. The above set of (Y_{OO}, Y_{FF}) represents a typical case and is employed extensively in the following analysis: the qualitative trends for other Y_{OO} and Y_{FF} values are similar. The thickness of the radiative loss zone is 0.04 for all values of N_R and the separation distance of the loss zone from the stoichiometric flame location is zero. We observe that the flame temperature profile is uniformly lowered as the value of N_R increases. Also, the flame temperature peak moves toward the fuel wall as the value of N_R is increased. The drop in flame temperature, as well as the shift of the peak, become more prominent for higher values of N_R . For a value of N_R greater than 383, we do not obtain a steady state temperature profile, indicating the occurrence of a radiative extinction. This maximum, or upper

bound, for N_R is then defined as $N_{R_{extinction}}$, i.e., $N_{R_{extinction}}=383$ for this case. We also note from Figure 4 that there is a change of slope of the temperature profile in the radiative loss zone for higher values of N_R , i.e., between Z_{R-} and Z_{R+} .

Figure 5 shows the nondimensional reaction rate term $((1+\phi)Dr)$ for the same situation. We observe that the reaction rate profile collapses for increasing N_R values. The reaction rate peak also moves towards the fuel side; this movement becomes more conspicuous for higher values of N_R . We notice that the reaction rate profile has managed to move nearly beyond the rightmost side of the radiation loss zone (indicated by the dashed lines at Z_{R-} and Z_{R+}) for the highest value of N_R .

We now focus on the temperature and species profiles for the situation when $N_R=383$ for the above case, i.e., at the brink of extinction. Figure 6 also shows the temperature and species profiles for the same flame for an infinite reaction rate. We notice that when $N_R=383$, the slope of the y_O profile is quite different from its IRR counterpart. On the other hand, the slope of the y_F profile follows the IRR y_F profile closely until a Z -value of about 0.3, when its slope starts decreasing. This plot therefore demonstrates explicitly the contrast between the IRR situation and the finite chemistry situation with appreciable radiative losses. The migration of the peaks of temperature and reactivity profiles is striking. Also, an abrupt change of the temperature profile seems to take place in the zone of radiative losses, i.e., between Z_{R-} and Z_{R+} .

We add for emphasis that from the strictly physical viewpoint, the finite-rate solution has attained a rather extreme form, since the reaction zone has almost completely propagated through the loss zone. In Figure 6, we see that the loss zone is now on the oxidizer side of the reaction rate profile. As we shall see, extreme cases like this are not the norm. They are also physically

unrealistic, though mathematically permissible in our simplified model with a prescribed heat loss function.

We illustrate the details of the flame structure in Figure 7, where we plot the contributions of the different terms in the energy equation when the steady state condition has been achieved. The loss term is given by $(N_R/\bar{s}_0) \text{sech}^2(B(Z-Z_R))$ and the diffusion term, as in equation (9), is $(1/\bar{s}_0^2)\tau_{ZZ}$. We have already noted from Figure 5 that for $N_R=383$ the reaction rate profile has penetrated through the radiative loss zone. Figure 7 indicates that the diffusion term recovers the radiative losses almost entirely and the reaction term doesn't contribute to the diffusion term in such a recovery process. This represents a completely different physical problem, when the radiative loss term exists on the oxidizer side of the primary reaction zone (flame). This result is, as already mentioned, clearly in conflict with our hypothesis that the heat losses take place on the fuel side of the flame due to flame-generated particulates. This occurs because our hypothetical radiative loss profile is simply a prescribed function in Z , and as such, it does not contain any mechanisms for loss-zone movement as the temperature and species profiles change, as a real soot zone invariably must.

In order to observe the effect of a thicker loss zone, we now increase ΔZ_R to a value of 0.1, see Fig. 8. We notice that the drop in the temperature profile is more significant in this case and the flame extinguishes at a lower value of the radiation number, viz., for $N_R=132$. We use this opportunity to note that $(N_R\Delta Z_R)_{ext}$ is approximately 14.2 for the first case and 13.2 for the second case. As shown in Wichman and Ray [14] for the simple top-hat loss profile, it appears the extinction results are best correlated with the function $N_R\Delta Z_R$, although the proper method of evaluating ΔZ_R is not as straightforward as our estimate suggests. The

correct method of evaluating ΔZ_R is discussed later in the article.

Next, we consider the situation when the left-most side of the loss zone is sufficiently removed from Z_f for a flame with $Y_{OO}=0.6$ and $Y_{FF}=0.8$. The thickness of the loss zone is $\Delta Z_R=0.06$ and the separation distance, Δ , is 0.1 in this case. Figure 9 shows that the flame temperature decreases with increasing N_R . Here, the movement of the peak nondimensional flame temperature is not pronounced, though it does move toward the fuel side. Correspondingly, Figure 10 shows the variation of the reaction term, $(1+\phi)Dr$, for increasing values of N_R . As mentioned for the preceding cases, therefore, the reaction zone does not always propagate through the loss zone. A sufficient separation and magnitude of the loss term appear sufficient to block the through-transit.

We note that the reaction rate peak is always to the left of the temperature peak, i.e., $Z_f < Z_r < Z_\tau$. This is in accordance with the results obtained for pure diffusion flames without radiative losses [9], as discussed before.

Figure 11 is an extinction plot for the case when $\Delta Z_R=0.06$ and $\Delta=0$. Extinction values of N_R are plotted as a function of Z_p , the theoretical flame location in the mixture fraction coordinate. We notice that for a given value of the oxidizer mass fraction at the wall, $(N_R)_{extinction}$ increases as Z_f is decreased. A decrease in Z_f implies an increase in ϕ , which, for a given Y_{OO} , produces an increase in Y_{FF} . As Y_{FF} increases, the reaction rate becomes more vigorous and it becomes more difficult to extinguish the flame through radiative losses. This explains the nature of the curves that we obtain on the extinction plot. Also, for the same value of Z_p i.e., for the same value of ϕ , a lower value of Y_{OO} indicates a correspondingly smaller value of Y_{FF} and hence, the reaction rate also becomes smaller in

magnitude. It is then easier to extinguish the flame. This explains why the curves in Figure 11 all shift toward the left for decreasing values of Y_{OO} .

Our focus is next shifted to some quantities of practical interest. We evaluate the heat transfer to the wall from flames with the same stoichiometry ($Y_{OO}=0.6$ and $Y_{FF}=0.8$) but with different thicknesses of the radiative loss zones and for different separation distances Δ from Z_f . Let $Q_{W,O}$ denote the heat transferred to the oxidizer wall by the flame per unit surface area of the wall. We reckon that the oxidizer wall will have a stronger effect on the flame than the fuel wall owing to the proximity of the flame to the oxidizer wall. The flame transfers heat to the oxidizer wall by means of both conduction and radiation, and hence,

$Q_{W,O} = Q_{W,O,cond} + Q_{W,O,rad}$ where the conduction flux is $Q_{W,O,cond} = -\lambda(dT/dx)|_{x=L}$ and the radiative flux is $Q_{W,O,rad} = 0.5 \times \int_0^L (dq_R/dx) dx$. We assume that half of the radiative losses travel to each wall: this assumption is reasonable in the thermally-thin limit we consider here. We

can transform the expressions for $Q_{W,O,cond}$ and $Q_{W,O,rad}$ to the Z coordinate and normalize $Q_{W,O}$

by the reference conductive flux $\lambda_o(T_f - T_o)/L$. The normalized

$\bar{Q}_{W,O} = (1/\bar{s}_o) d\tau/dZ|_{z=0} + 0.5 \times (1/\bar{s}_o) N_R \int_0^1 (1/\bar{s}_o) (d\bar{q}_R/dZ) dZ$. The quantity $\bar{Q}_{W,O} \bar{s}_o$ is plotted in

Figure 12. It is apparent that the heat transfer characteristics do not depend strongly on the separation distance Δ , and consequently, we see four reasonably distinct groups of curves

corresponding to loss zones of four different thicknesses. However, as is evident from the plot, the separation distance Δ does become important for higher values of N_R close to

extinction. We will notice that, nearing extinction, the flame attempts to reduce the heat losses to the wall as much as possible. Also, the value of N_R required for extinction is higher when

the heat loss zone is very thin, as intuitively obvious.

We also plotted \bar{Q}_{w, σ_0} as a function of the quantity $N_R(2/B)$. Figure 13 clearly shows that the quantity $N_R(2/B)$, which is approximately the value of the integral $\int_0^1 N_R \text{sech}^2[B(Z-Z_R)] dZ$, is able to collapse the wall heat transfer data except very near extinction. Thus, when plotted against $N_R(2/B)$, \bar{Q}_{w, σ_0} does not reveal any appreciable dependence on either the separation distance Δ or even the thickness of the loss zone ΔZ_R . The correlation in the straight-line region is given approximately by $\bar{Q}_{w, \sigma_0} = 1.9(N_R(2/B)) + 5.3$, which is reasonably accurate until the curves make their final turn toward the abscissa.

Another quantity of practical interest is the radiative fraction χ , given by the ratio q_{rad}/q_{Total} . The quantity q_{rad} is the integral of the radiative loss term, i.e., $\int_0^1 N_R \text{sech}^2[B(Z-Z_R)] dZ$ and q_{Total} is the integrated value of the reaction rate in mixture fraction space, i.e., $\int_0^1 (1+\phi) D r dZ$. From Figure 14 we notice that q_{Total} decreases with increasing values of N_R . This happens because with increased intensity of the radiative loss zone, reaction rate values decrease as already observed in Figures 5 and 10. For thicker loss zones, the drop in q_{Total} with increasing values of N_R is more rapid.

We have already noted in section 2.2 that the integral of the radiative loss term profile is approximately $(N_R \bar{s}_0)(2/B)$. Hence, it is of interest to plot the total heat release q_{Total} as a function of the quantity $N_R(2/B)$. The result is shown in the Figure 15. Figure 15 indicates that the quantity $N_R(2/B)$ characterizes the total heat release rate very well and the curves for different loss zone thicknesses virtually collapse on one another except for large values of N_R close to extinction. The correlation in the linear region is given by $q_{Total} = -15.25N_R(2/B) + 168$. The constants in this formula depend on the global stoichiometry.

Figure 16 illustrates the variation of χ as a function of N_R for different thicknesses

of the loss zones and for $\Delta=0$. We observe that χ increases with increasing N_R for a flame with a given loss zone thickness. The integrated quantity q_{rad} increases with N_R and, since correspondingly the q_{Total} values decrease, χ , which is a ratio of the above quantities, increases. In order to produce a given value of χ , a higher value of N_R is required for a flame with a thinner loss zone. Similar to the study of q_{Total} , we plot χ as a function of $N_R(2/B)$ in Figure 17. It is clear from the figure that the use of $N_R(2/B)$ collapses the data very well except close to extinction. Here, the correlation in the linear segment is $\chi=0.038N_R(2/B)$; once again, the multiplicative constant must be a function of global stoichiometry. Figure 18 shows the variation of the drop in flame peak temperature, $\Delta\tau_f$, as a function of the radiative fraction χ . If we denote the maximum temperature by τ_f , then $\Delta\tau_f$ is defined as $1-\tau_f$. We recall that the temperature has been normalized in such a way that the peak nondimensional temperature for the infinite reaction rate situation always has the value of unity, regardless of the oxidizer and fuel mass fractions. Thus, $\Delta\tau_f$ represents the drop in peak temperature for finite rate chemistry and radiative loss situation, in comparison to the IRR situation. The increase in $\Delta\tau_f$ with χ was almost linear for smaller values of χ , with $\Delta\tau_f \approx \chi + 0.1$ as the correlating function. However the curves for the different loss zone thicknesses diverged from one another for higher values of χ .

It has been previously mentioned (section 2.2) that the results for the $sech^2$ heat loss profile can be compared with the results of Wichman and Ray [14] for the top-hat profile. However, the thickness ΔZ_R of the top-hat profile must be chosen to be $2/B$, where the value of B is determined from the choice of the thickness of the $sech^2$ profile. For example, when $(\Delta Z_R)_{sech^2}$ is chosen to be 0.06, the constant $B=99.7$ and consequently

$(\Delta Z_R)_{top-hat} = 2/99.7 \approx 0.02$. As shown in [14], both analytical and numerical methods were used to determine the extinction value of N_R for the top-hat profile. Here, we compare analytical and numerical results for the top-hat profile with the numerical solutions for the $sech^2$ profile. Figure 19 depicts the extinction N_R values plotted as a function of Z_f when $Y_{O_2} = 0.7$, $(\Delta Z_R)_{sech^2} = 0.06$, $(\Delta Z_R)_{top-hat} = 0.02$ and $\Delta = 0.1$. The direction of increasing Y_{FF} has also been indicated on the plot. The numerical solutions reveal that the $sech^2$ and the top-hat profiles produce very similar $N_{R,extinction}$ values. This indicates that the integrated value of the radiative loss term is the quantity which determines the extinction N_R value. The extinction N_R values obtained by analytical method are quite different from the numerical solution. However, inspection of the curves depicted in Figure 19 shows that the ratio of the analytically obtained values to the numerical solution is very nearly ($\pm 1.5\%$) 3.8 for all the Z_f values plotted in Figure 19, exactly as in [14]. This indicates that a simple modification of the analytical formula of [14] based on the inclusion of a correction factor should yield close correspondence between the analytical and numerical results. Thus, we use

$$[N_R(2/B)]_{ext} = \frac{C}{Z_f(1-\theta/2)} \frac{1}{\beta} \ln \left[\frac{4D_o Z_f^2 (1-Z_f)^3}{(b_E \beta)^3} \right], \quad (17)$$

where D_o is the Damköhler number defined under Equation (11), b_E is the extinction value of the reduced Damköhler number (see [14]) and $\theta = Z_{R+} + Z_{R-}$, which we write as $\theta = 2Z_R$ after using $Z_{R+} = Z_R + \Delta Z_R/2$, $Z_{R-} = Z_R - \Delta Z_R/2$. In other words, Z_R is the value of the heat loss zone peak. With $C = 1/3.8$ this formula correlates the numerically-derived data of Fig. 19 within line width. This multiplicative factor will depend on the global stoichiometry, of course.

5. CONCLUSIONS

We investigated the influence of a simple and hypothetical heat loss zone on a pure diffusion flame in detail. The loss profile was of the form of a *sech*² given by equation (12) and we varied the intensity and the width of the loss zone to study the diffusion flame response. The loss zone was postulated to lie always on the fuel side of the ideal Burke-Schumann flame. The location of the loss zone on the fuel side relative to the ideal flame location Z_f was also varied. In all situations, the increase of the radiation number N_R results in a movement of the flame toward the fuel side. We found that for thin loss zones located close to Z_f , the reaction zone may even migrate through the flame to the fuel side of loss zone for significantly high values of N_R . In such a situation the loss zone now lies on the oxidizer side of the flame, contrary to our initial postulate. This happens because our hypothetical loss zone is static and contains no mechanism for movement. The reaction rate profile, on the other hand, is free to move and hence locates itself on the fuel side of the loss zone in certain cases.

Extinction plots were generated for different flames for given loss zone thicknesses (ΔZ_R) and given separation distances (Δ). The plots indicated that for a given Y_{OO} , an increase in Y_{FF} results in higher values of extinction radiation number, N_R .

Nondimensional heat transfer rates to the oxidizer wall were also investigated. The results indicated that the separation distance Δ did not have a significant influence on the wall heat transfer characteristics.

The total heat release in the combustion process, q_{Total} , was found to decrease with increasing values of N_R and the rate of decrease was quite rapid for thicker loss zones. It was found that the quantity $N_R(2/B)$ characterizes q_{Total} very well and the curves for the

different loss zone thicknesses and separation distances all collapse onto one another except near extinction. A correlation was produced in the linear region. We expect that the correlation constants depend upon the flame stoichiometry.

Investigation of the radiative fraction showed that χ increases with increasing values of N_R and the rate of increase is steeper for thicker loss zones. The flame, however, extinguishes at a larger value of χ for loss zones which are relatively thin. The quantity $N_R(2/B)$ collapses the q_{Total} and radiative fraction values very well except near flame extinction. A linear correlation formula was produced whose coefficients vary with global flame stoichiometry. The detailed determination of these coefficients will be the subject of a future work. The decrease in the flame temperature was nearly linear with radiative loss fraction, as shown in Fig. 18. The linearity, away from near-extinction, of all of these results is very encouraging for the development of a simplified description of soot radiation in flames. Once a suitable N_R is defined and an estimate is made of the soot layer thickness $2/B$ in mixture-fraction space, correlations resembling those of Figs. 13, 15, 17, 18 can be generated for the important overall heat-transfer quantities. The estimation of the soot-layer thickness will be the subject of a future work.

Finally, we demonstrated that the extinction formula derived in Ref. [14] could be easily modified to suit this *sech*² model by replacing the top-hat loss zone thickness with $2/B$ for large B . The hop-hat and *sech*² profiles thus modified produce exactly the same $N_{R_{extinction}}$ vs Z_f curve, see Fig. 19. The correlation with the analytical formula derived in [14] is given by equation (17) with the new effective loss-zone thickness $2/B$. We expect that the multiplicative empirical constant (here 3.8), will depend fairly weakly on the global stoichiometry. Many cases must be examined in order to determine this dependence.

ACKNOWLEDGEMENT

This work was funded by the NASA microgravity combustion division, contract # NAG3-1271, monitored by Kurt Sacksteder. We are very grateful for this support.

NOMENCLATURE

a	Constant in asymptotic formulation defined by Eq. (35.i)
a_p	Planck mean absorption coefficient
A	Pre-exponential factor
b	Reduced Damköhler number defined by Eq. (35.iii)
b^*	Reduced Damköhler number with zero heat losses
c	$O(1)$ constant in asymptotic formulation, see (Eq. (35.ii))
D, D_o	Damköhler number; Damköhler number with no heat losses
D_o, D_F	Diffusion coefficients for oxidizer, fuel
E	Activation energy
f_v	Soot volume fraction
h_i	Specific enthalpy of species i
h	Rescaled enthalpy loss, $h = \beta H(Z_{R-}) $
H	Enthalpy defect, $H = \tau + y_o + y_F - 1$
H_o	Enthalpy defect with zero heat losses, $H_o = 0$
L	Combined heat loss; distance between fuel and oxidizer walls
N_R	Radiation number, see Sec. 2.4
\bar{q}_R	Nondimensional radiant energy flux, see (Eq. (1) and above Eq. (2))
Q_F	Heat release per unit mass of fuel
\bar{Q}_F	Nondimensional heat release
r	Nondimensional reaction term, $r = y_o y_F \exp[-\beta(1-\tau)/(1-\alpha(1-\tau))]$
R	Universal gas constant
s, s_o	Mass coordinate, $s = \int_o^x \rho dx$, $s_o = \int_o^L \rho dx$

\bar{s}_o	Nondimensional mass coordinate, $\bar{s}_o = s/s_o$
S	Redefined dependent variable, $S = \tau - H = 1 - (y_o + y_f)$
T, T_f, T_o, T_R	Temperature (flame, ambient, radiation zone)
u	Flow velocity
$U_o(Z)$	Heaviside step function
w	Reaction term, $w = \rho A Y_o Y_f \exp(-E/RT)$
x	Spatial coordinate
y_f, y_o	Rescaled fuel, oxidizer mass fractions
Y_f, Y_o	Fuel, oxidizer mass fractions
Z	Physical coordinate, $Z = 1 - \bar{s}$, coincides with mixture fraction
Z_{R+}, Z_{R-}, Z_R	Z-values at right, left, middle of radiation-loss zone

GREEK

α	Enthalpy ratio, $\alpha = 1 - T_o/T_f$
β	Zeldovich number, $\beta = \alpha E/RT_f$
ΔZ_R	Radiation-loss zone thickness, $\Delta Z_R = Z_{R+} - Z_{R-}$
ϵ	Small dimensionless parameter
η	Rescaled mixture fraction, see above Eq. (31)
θ	Sum of Z_{R+} and Z_{R-} , $\theta = Z_{R+} + Z_{R-}$
λ	Thermal conductivity
ξ	Nondimensional physical coordinate, $\xi = \bar{s}$
ρ	Density

- σ Stefan-Boltzmann constant
- τ Nondimensional temperature, $\tau = (T - T_\infty) / (T_f - T_\infty)$
- ϕ Global equivalence ratio
- Φ Scaled value of S in reaction zone, see above Eq. (31)

REFERENCES

- [1] J.D. Felske and C.L. Tien. *Combustion Science and Technology*, 7:25, 1973.
- [2] G.H. Markstein. In *Sixteenth Symposium (International) on Combustion*, page 1407, The Combustion Institute, Pittsburgh, 1976.
- [3] C.L. Tien and S.C. Lee. *Progress in Energy and Combustion Science*, 8:41, 1982.
- [4] W.L. Grosshandler and J.P. Vantelon. *Combustion Science and Technology*, 44:125, 1985.
- [5] S.H. Chan, X.C. Pan, and M.M.M. Abou-Ellail. *Combustion and Flame*, 102:438, 1995.
- [6] J.P. Gore and J.H. Jang, *Journal of Heat Transfer*, 114:234, 1992.
- [7] Y.R. Sivathanu and J.P. Gore, *Combustion and Flame*, 97:161, 1994.
- [8] W.L. Grosshandler and A.T. Modak. In *Eighteenth Symposium (International) on Combustion*, page 601, The Combustion Institute, Pittsburgh, 1981.
- [9] I.S. Wichman. *An Introduction to Combustion Modeling Using High-Activation-Energy Asymptotic (AEA) Methods*, CRC Press, 1993.
- [10] F.A. Williams. *Combustion Theory*, The Benjamin/Cummings Publishing Company, Inc., 1985.
- [11] R.J. Santoro, T.T. Yeh, J.J. Horvath, and H.G. Semerjian. *Combustion Science and Technology*, 53:89, 1987.
- [12] I.S. Wichman, PhD thesis, Princeton University, 1983.
- [13] L.S. Tzeng, A. Atreya, and I.S. Wichman. *Combustion and Flame*, 80:94, 1990.
- [14] I.S. Wichman and A. Ray, submitted, 1996.

LIST OF CAPTIONS FOR FIGURES

- Figure 1: The problem geometry, including the diffusion flame (DF), the radiation (soot) zone and the porous diffusive walls at $x=0$ and $x=L$. The reactant influx is purely diffusive.
- Figure 2: Flame temperatures via simple correlation. Note that the maximum T_f for $Y_{FF}=0.25, 0.3$ occurs near $Y_{OO}=0.4$: we do not use these curves for this very reason.
- Figure 3: The sech^2 heat-loss profile showing the separation Δ between Z_f and Z_R , and our (preliminary) definition of ΔZ_R (which we shall subsequently modify).
- Figure 4: Influence of increasing N_R on the temperature distribution in a diffusion flame. Here the flame penetrates the loss zone, which is unrealistic unless oscillations occur. When $N_R > 383$, τ crashes everywhere to zero.
- Figure 5: Same as Fig. 4 for the reaction rate. Here the migration of the flame is immediately obvious.
- Figure 6: Profiles of τ, y_O, y_F and reaction rate for infinite and finite-rate cases, the latter just prior to extinction. Note that the y_F profile is virtually unchanged from its IRR value until inside the reaction zone.
- Figure 7: The flame structure for Fig. 4 at the brink of extinction.
- Figure 8: Influence on temperature field of increasing N_R on the same DF as Fig. 4 except the loss zone is 2.5x thicker, $\Delta Z_R=0.1$.
- Figure 9: Influence of non-zero initial displacement Δ between the loss zone and the DF (at Z_f). Here, the flame does not penetrate the loss zone before extinction.
- Figure 10: Same as Fig. 9 for the reaction rate. The right-ward movement in mixture fraction space is obvious.
- Figure 11: Extinction plot for $\Delta Z_R=0.06$ and zero initial displacement, $\Delta=0$. Along each curve, Y_{FF} increases as Z_f decreases. The largest Y_{FF} values have the highest $(N_R)_{ext}$ values.
- Figure 12: Total heat flux (nondimensional) to the oxidizer wall versus N_R .
- Figure 13: A replot of Fig. 12 with new abscissa $N_R(2/B)$. The correlation of the straight-line region is (heat flux) = $1.9N_R(2/B) + 5.3$.

- Figure 14: The total heat flux as a function of N_R for various loss-zone thicknesses and zero displacement, $\Delta=0$. As N_R increases, the integrated reaction rate decreases monotonically.
- Figure 15: Replot of Fig. 14 showing the collapse of the data to a single line except very near extinction.
- Figure 16: Radiant flux fraction versus N_R .
- Figure 17: A replot of Fig. 16 with abscissa $N_R(2/B)$ showing collapse of data to a single curve.
- Figure 18: The decrease in flame temperature versus radiant flux fraction shows a linear functional form that is virtually independent of the loss-zone width, ΔZ_R .
- Figure 19: Plot of $N_{R,ext}$ versus Z_f for the *sech*² loss profile and the previously-examined top-hat loss profile [14]. The close agreement between the numerical solutions indicates that the correlation with the analytical formula will be outstanding when the latter formula is multiplied by $(3.8)^{-1}=0.261$.

TABLE 1: FLAME TEMPERATURE VERSUS Y_{∞} DATA

Y_{∞}	0.211	0.233	0.247	0.276	0.329	0.432	0.533	0.727	1.0
T_f	2137	2230	2295	2385	2515	2684	2789	2919	3026

TABLE 2: PARAMTER VALUES.

Specific heat	C_p	1.35	J/kgK
Thermal diffusivity	α_0	1.24×10^{-4}	m^2/s
Fuel-oxidant mass ratio	ν	4.0	
Pre-exponential factor	A	5×10^7	$1/s$
Activation energy	E	121,841.7	$KJ/kmol$
Heat release	Q_f	11959.43	KJ/KgK

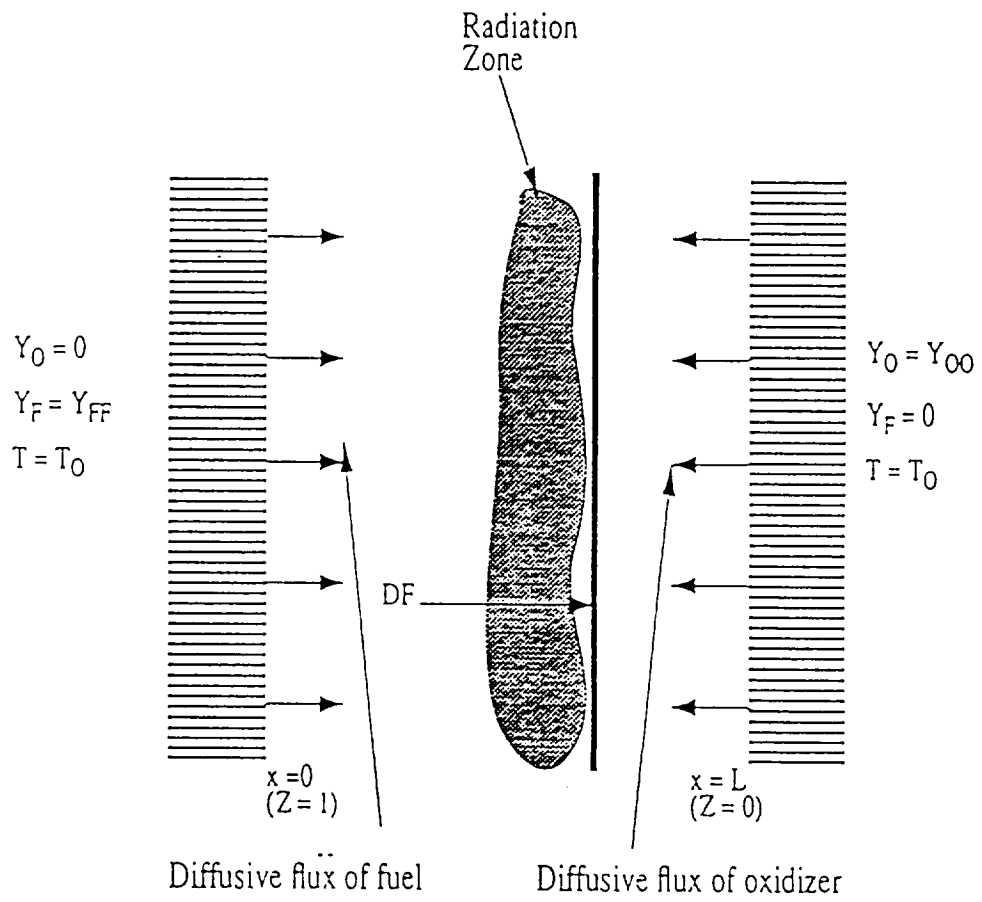


FIG. 1

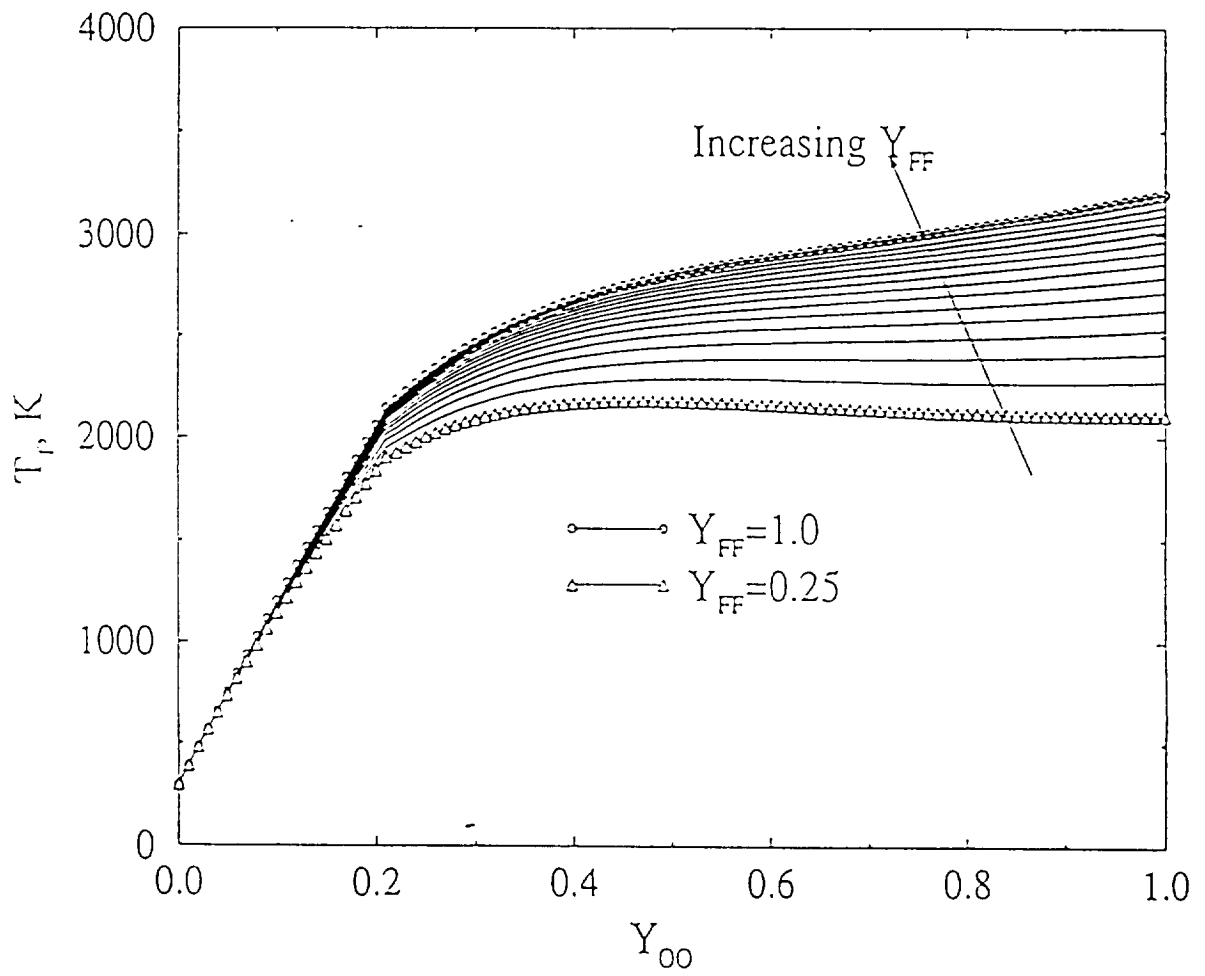


FIG. 2

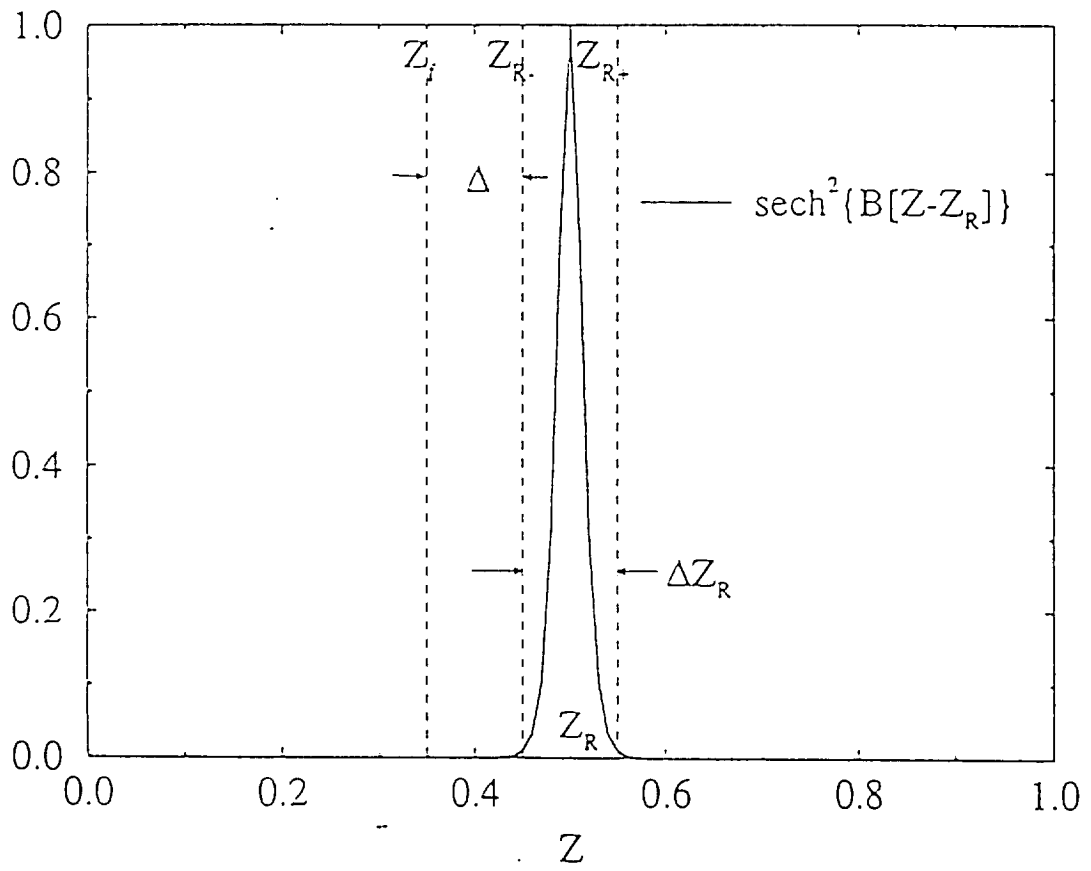


FIG. 3

$$Y_{O_2} = 0.6 \quad Y_{FF} = 0.8 \quad \Delta Z_R = 0.04 \quad \Delta = 0$$

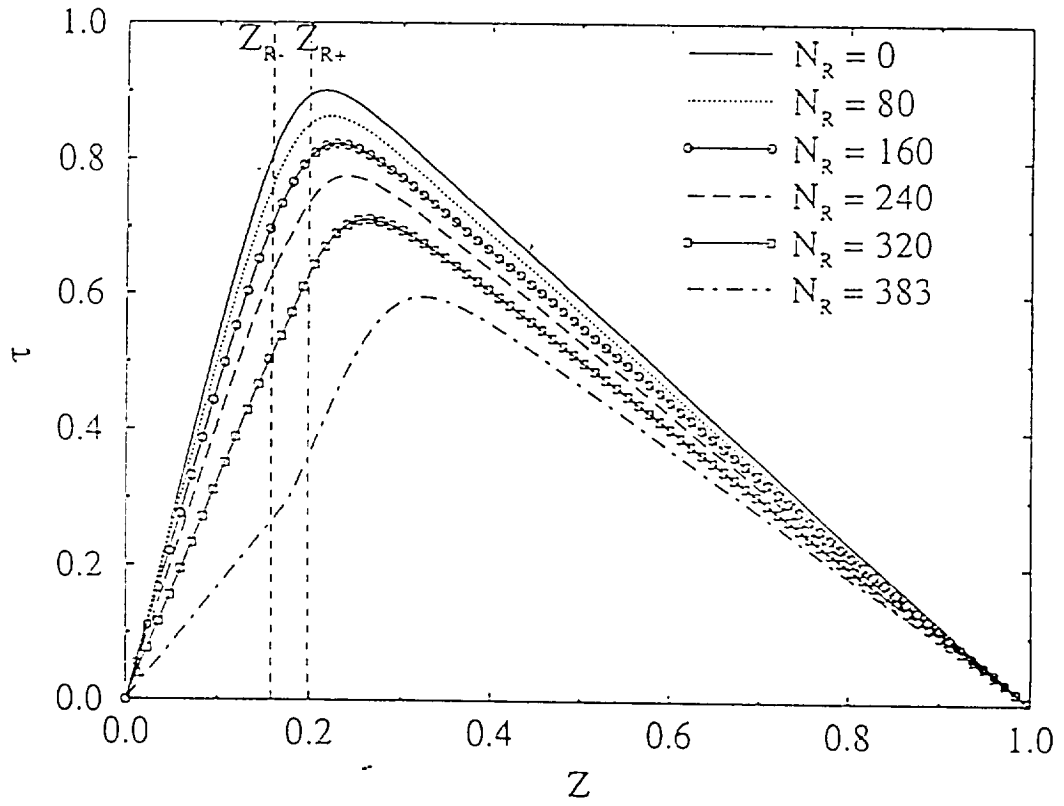


FIG. 4

$$Y_{OO}=0.6 \quad Y_{FF}=0.8 \quad \Delta Z_R=0.04 \quad \Delta=0$$

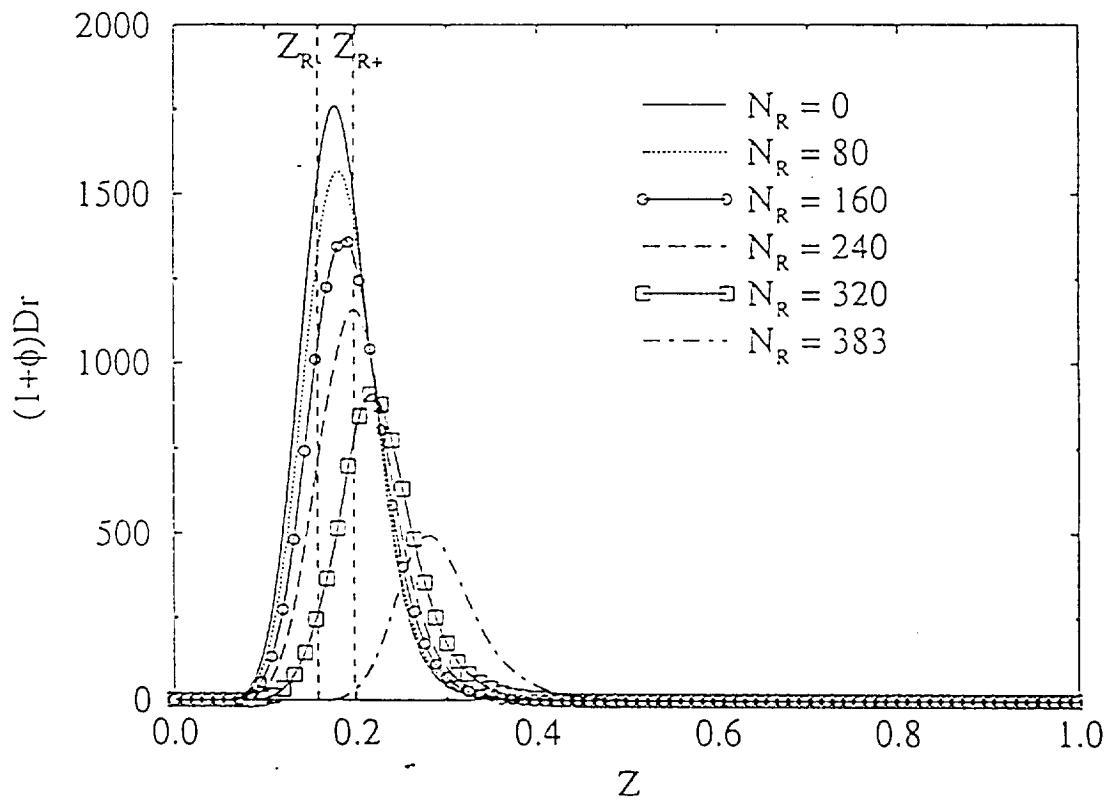


FIG. 5

$Y_{OO}=0.6$ $Y_{FF}=0.8$ $N_R=383$ $\Delta Z_R=0.04$ $\Delta=0$

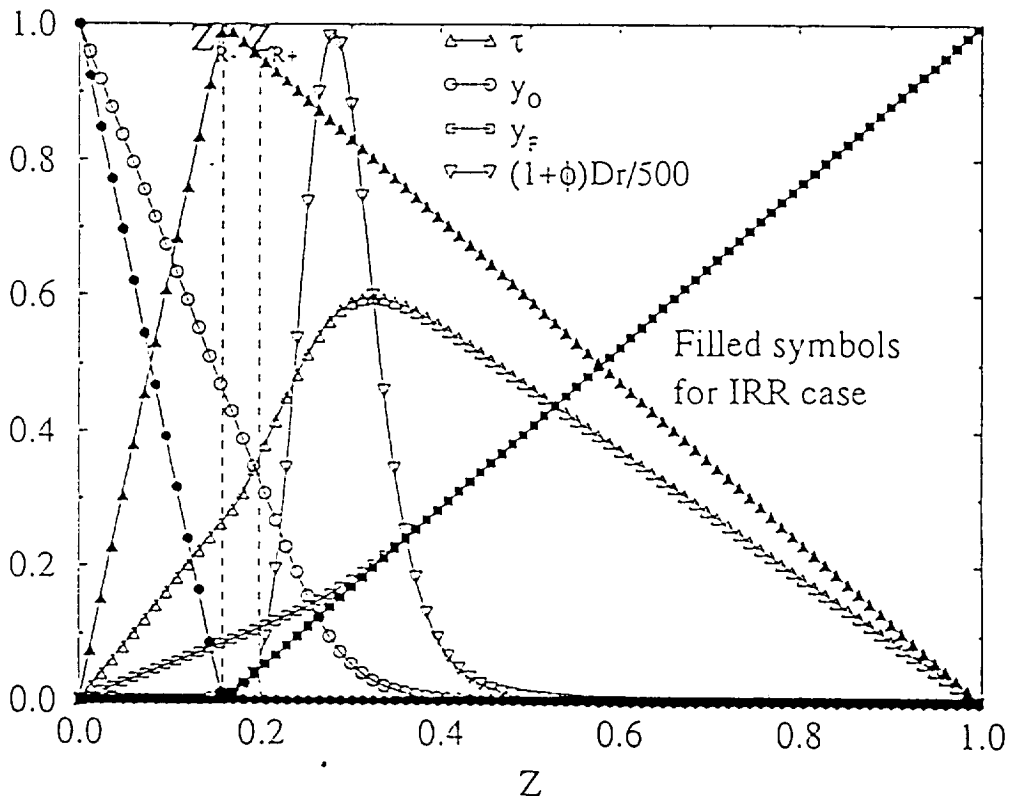


FIG. 6

$Y_{OO}=0.6$ $Y_{FF}=0.8$ $N_R=383$ $\Delta Z_R=0.04$ $\Delta=0$

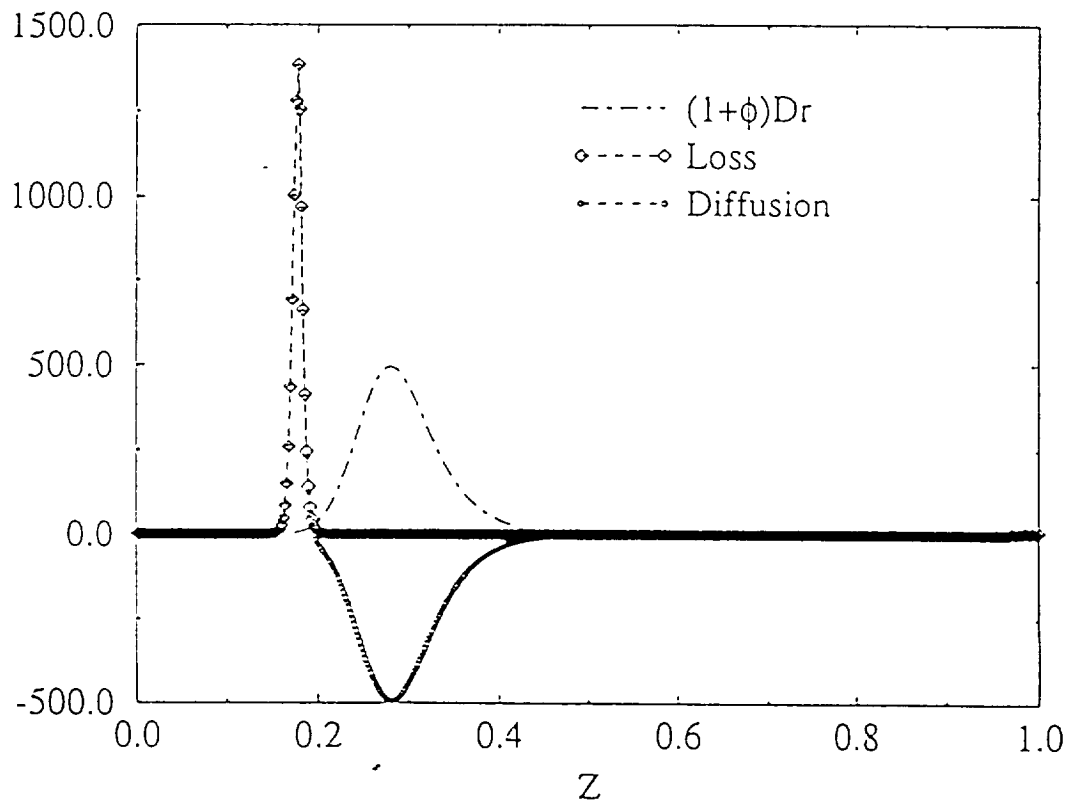


FIG. 7

$$Y_{00}=0.6 \quad Y_{FF}=0.8 \quad \Delta Z_R=0.1 \quad \Delta=0$$

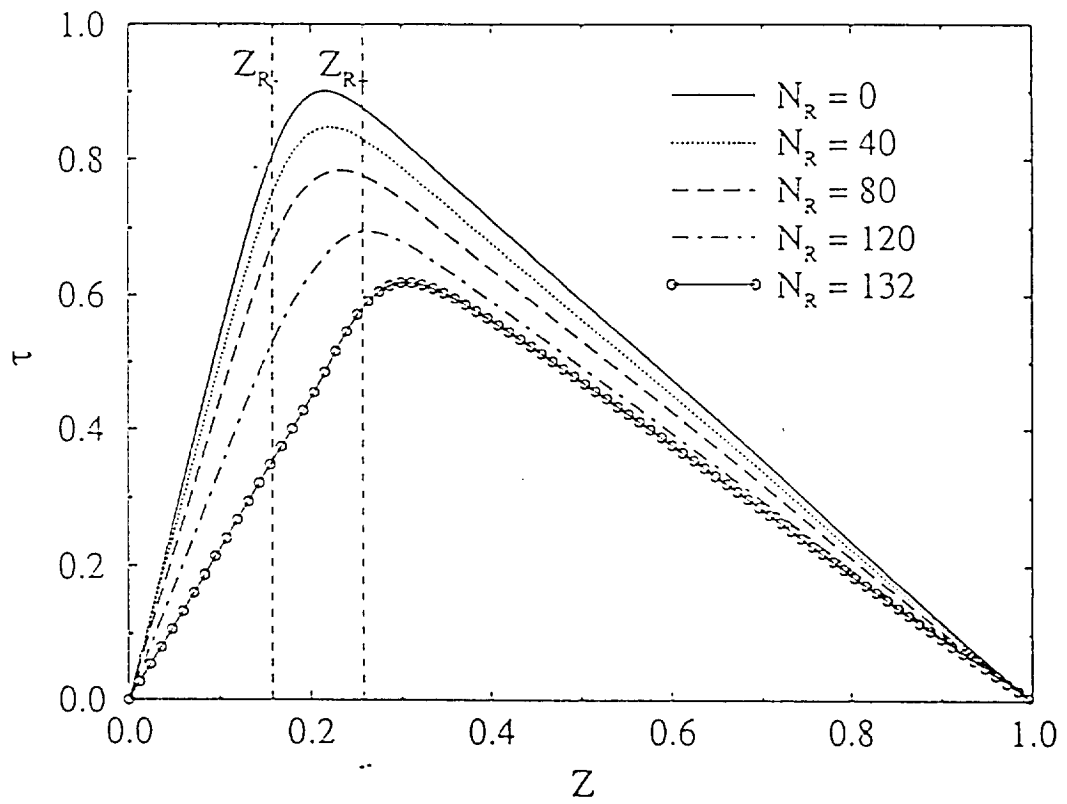


FIG. 8

$$Y_{00} = 0.6 \quad Y_{FF} = 0.8 \quad \Delta Z_R = 0.06 \quad \Delta = 0.1$$

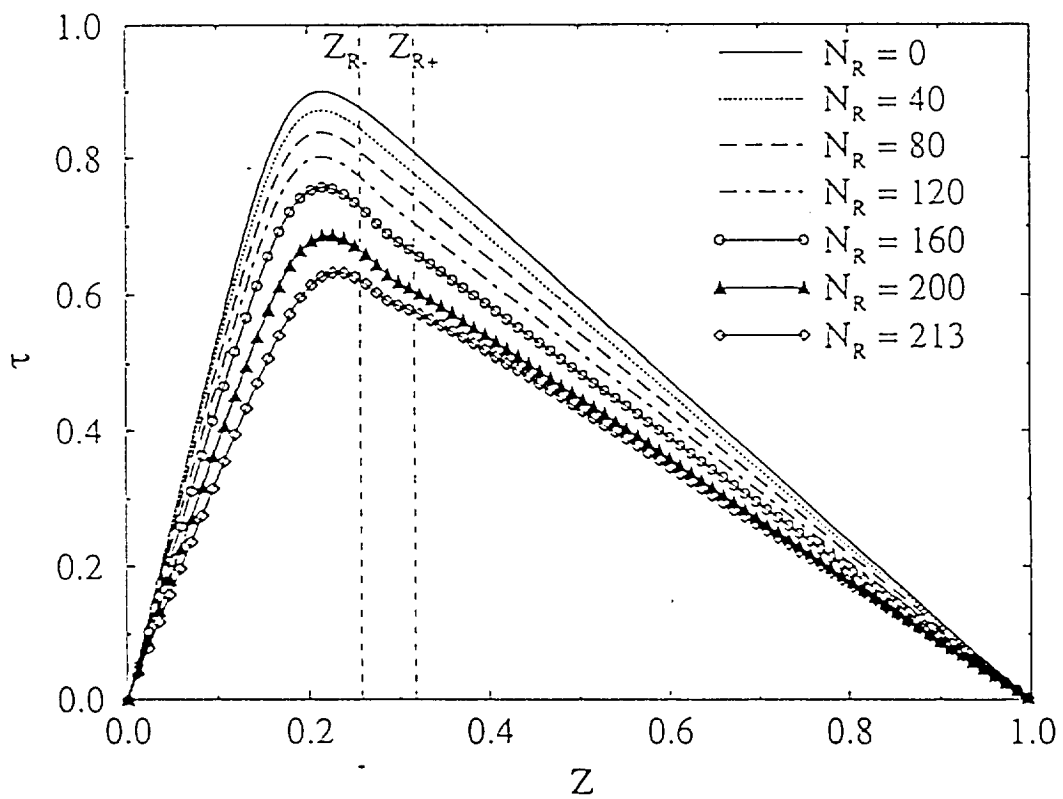


FIG. 9

$Y_{OO}=0.6$ $Y_{FF}=0.8$ $\Delta Z_R=0.06$ $\Delta=0.1$

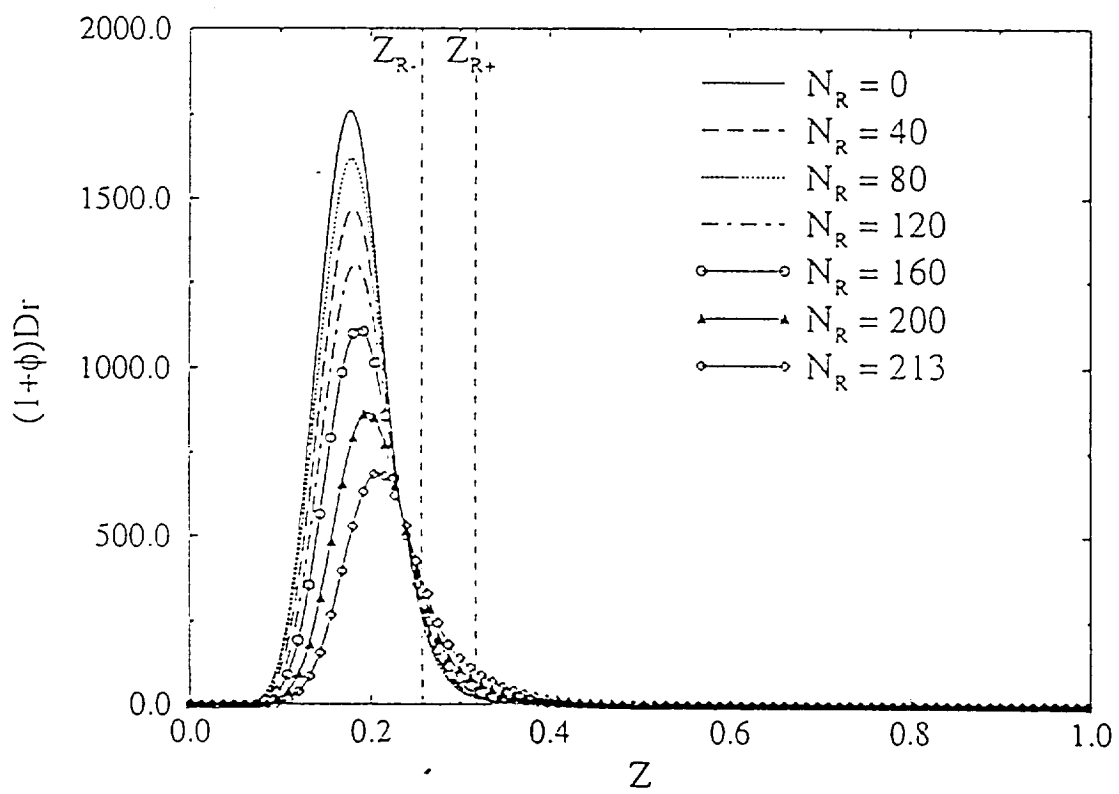


FIG. 10

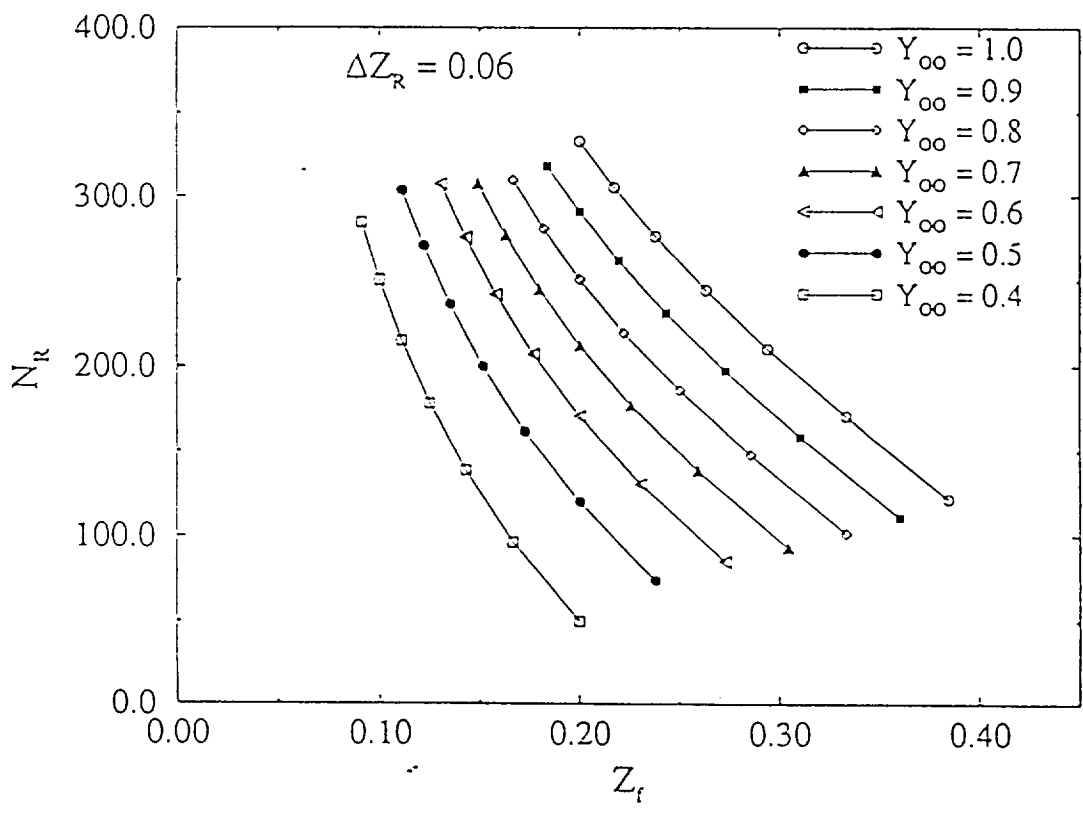


FIG. 11

$$Y_{OO} = 0.6 \quad Y_{FF} = 0.8$$

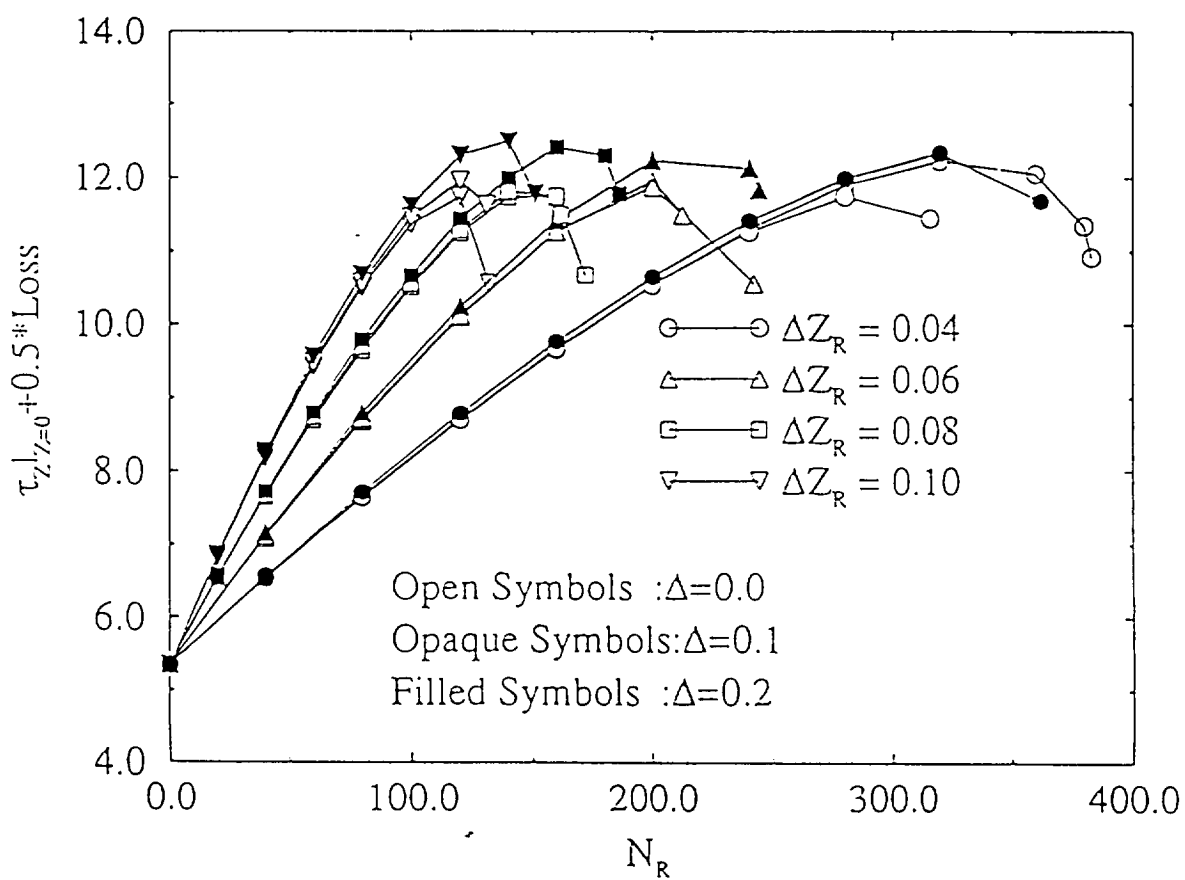


FIG. 12

$$Y_{\infty} = 0.6 \quad Y_{FF} = 0.8$$

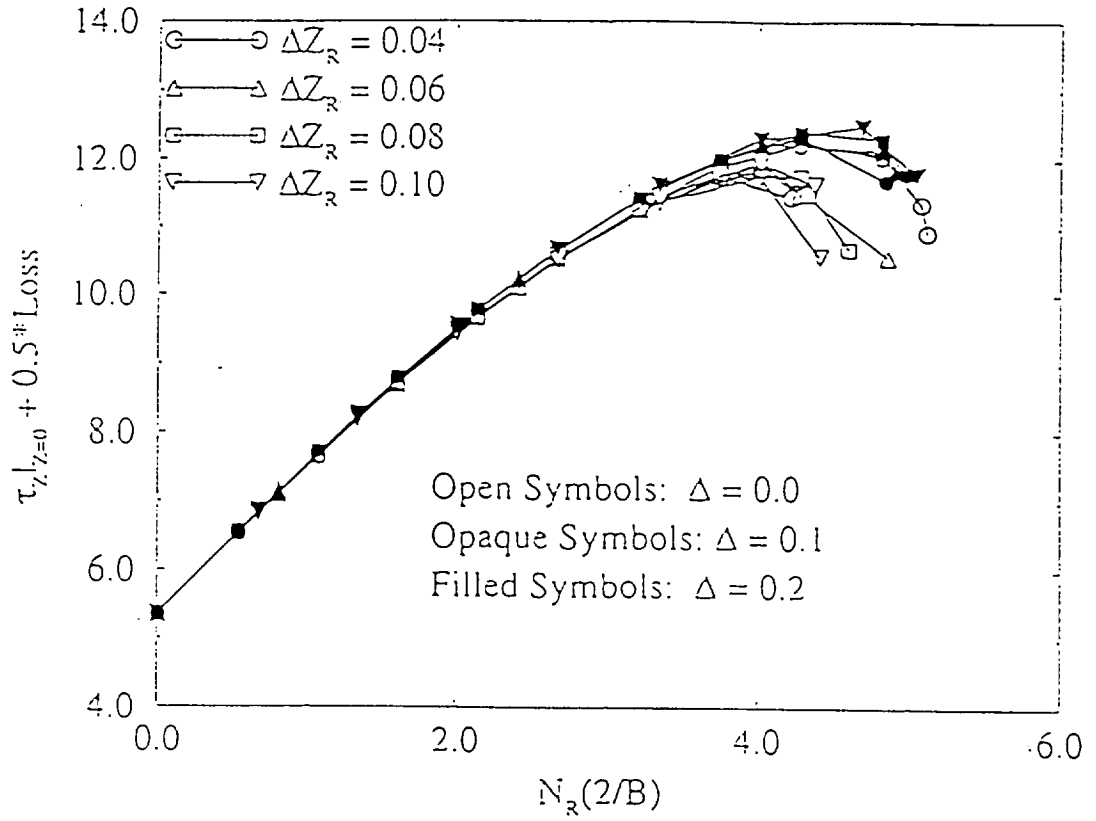


FIG. 13

$$Y_{OO} = 0.6 \quad Y_{FF} = 0.8 \quad \Delta = 0$$

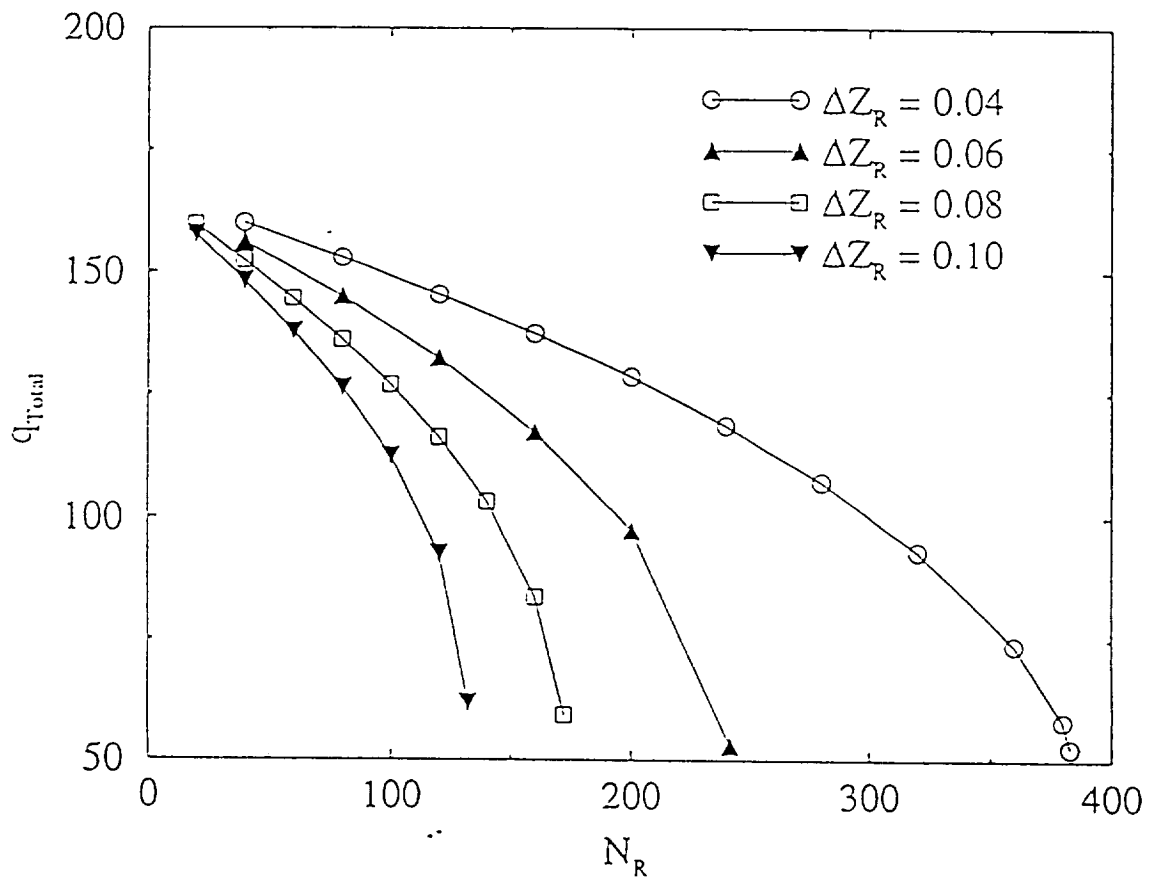


FIG. 14

$$Y_{\infty} = 0.6 \quad Y_{\infty} = 0.8 \quad \Delta = 0$$

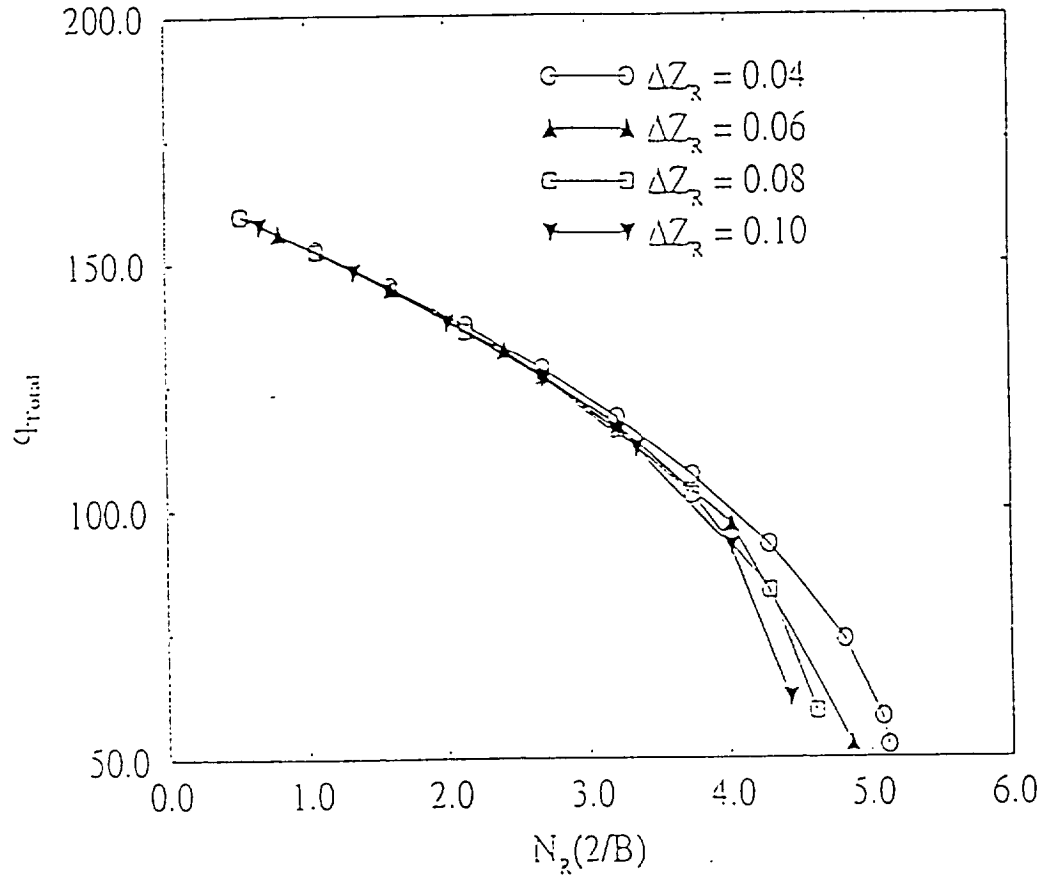


FIG. 15

$$Y_{OO} = 0.6 \quad Y_{FF} = 0.8 \quad \Delta = 0$$

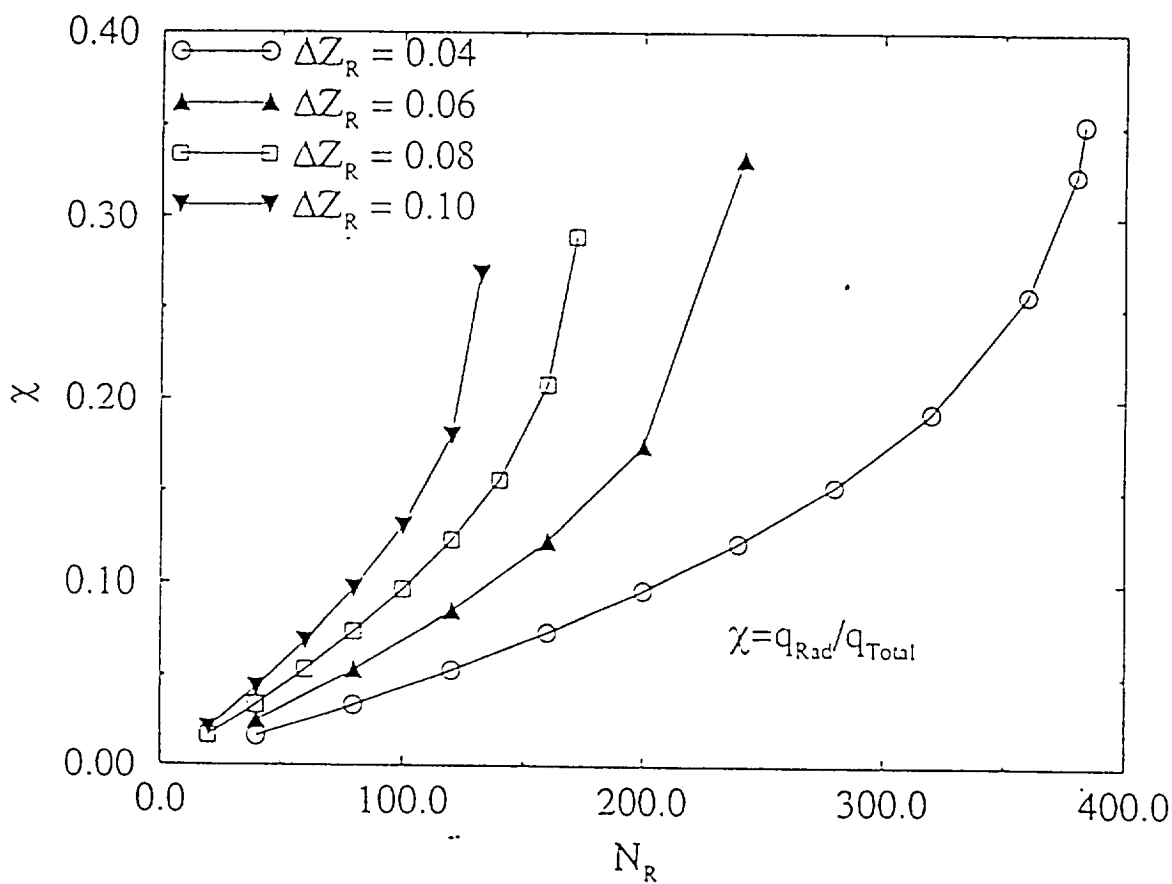


FIG. 16

$$Y_{\infty} = 0.6 \quad Y_{FF} = 0.8 \quad \Delta = 0$$

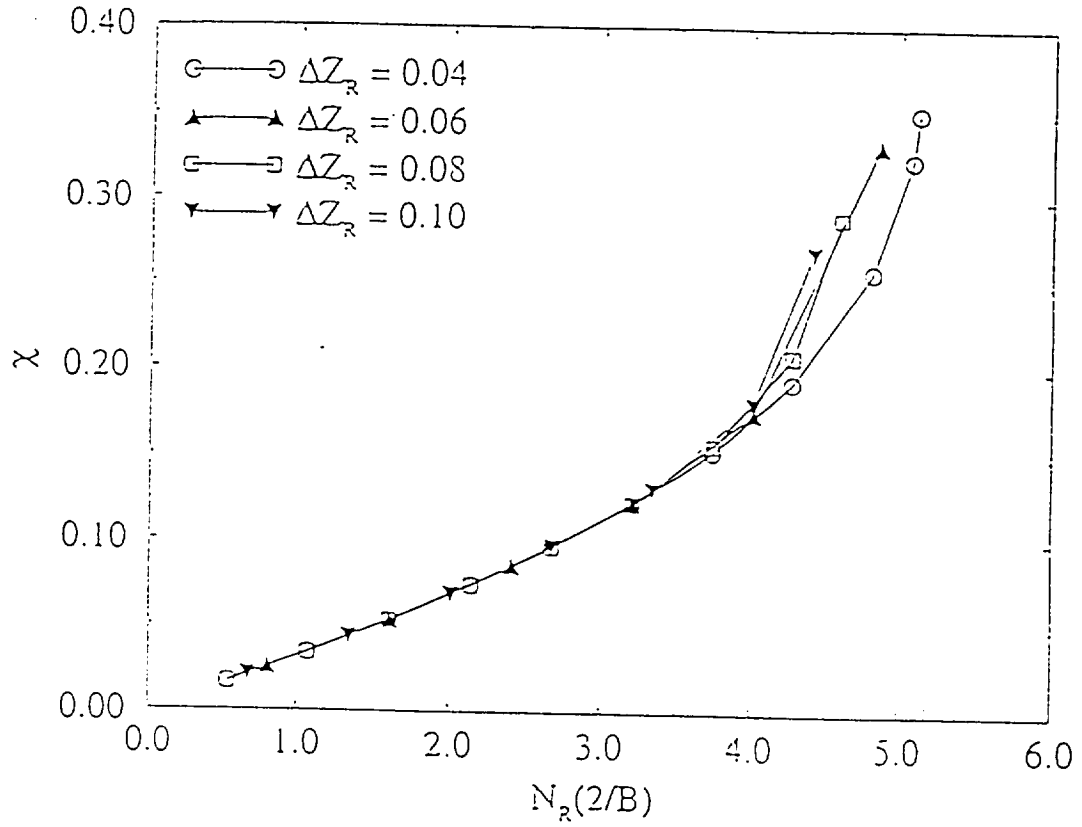


FIG. 17

$Y_{CO}=0.6 \quad Y_{FF}=0.8 \quad \Delta=0$

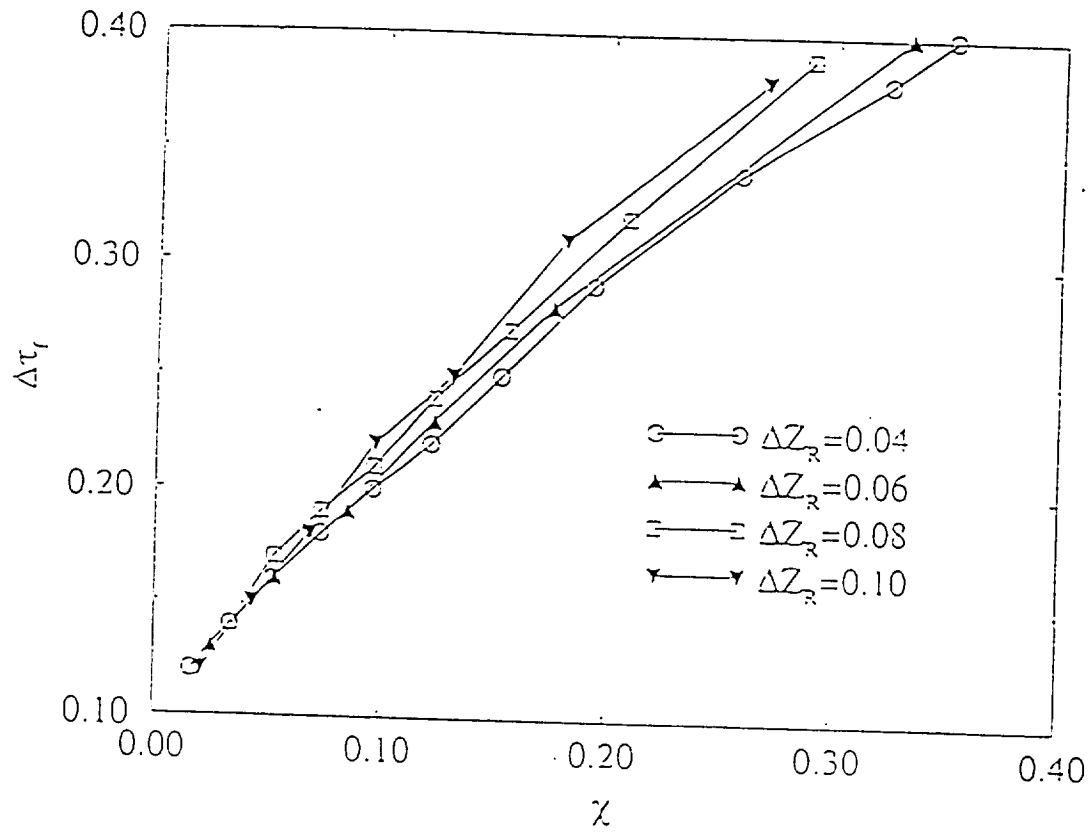


FIG. 18

$$Y_{\infty} = 0.7 \Delta Z_R = 0.06 \text{ (sech}^2\text{)}$$

$$\Delta Z_R = 0.02 \text{ (top-hat)} \Delta = 0.1$$

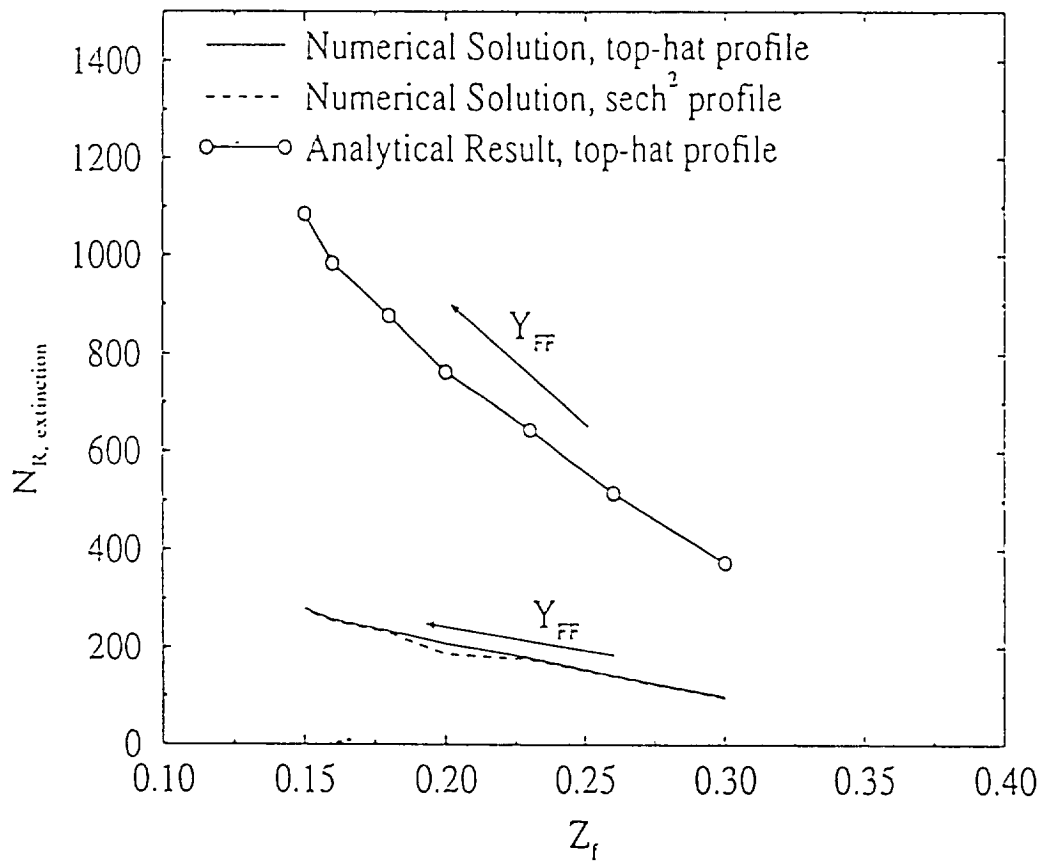


FIG. 19